RSC Advances

ROYAL SOCIETY OF CHEMISTRY

www.rsc.org/advances

TOC Image & Text:

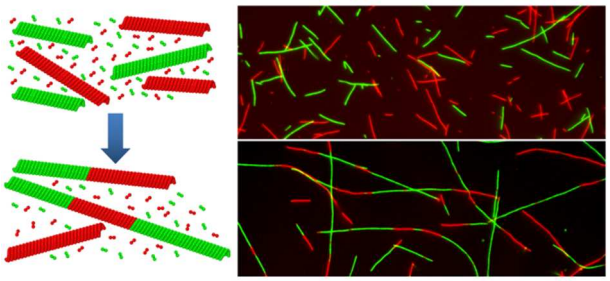

The intrinsic properties of microtubule filaments (e.g., biological nano-rods) direct their self-assembly into one-dimensional nano-arrays over extended timescales.

RSC Advances

ARTICLE

Directed self-assembly of 1D microtubule nano-arrays

Cite this: DOI: 10.1039/x0xx00000x

M. Bachand,[a] N. F. Bouxsein,[b] S. Cheng,[c,d] S. J. von Hoyningen-Huene,[b] M. J. Stevens,[c] and G. D. Bachand[b]

Received 00th January 2012,
Accepted 00th January 2012

DOI: 10.1039/x0xx00000x

www.rsc.org/

Microtubules (MTs) are biological polymer filaments that display unique polymerization dynamics, and serve as inspiration for developing synthetic nanomaterials that exhibit similar assembly-derived behaviours. Here we explore an assembly process in which extended 1D nano-arrays (NAs) are formed through the directed, head-to-tail self-assembly of MT filaments. In particular, we demonstrate that the elongation of NAs over time is due to directed self-assembly of MTs by a process that is limited by diffusion and follows second-order rate kinetics. We further described a mechanism, both experimental and through molecular dynamics simulations, where stable junctions among MT building blocks are formed by alignment and adhesion of opposing filament ends, which is followed by formation of a stable junction through the incorporation of free tubulin and the removal of lattice vacancies. The fundamental principles described in this directed self-assembly process provide a promising basis for new approaches to manufacturing complex, heterostructured nanocomposites.

Introduction

The spontaneous self-assembly of molecular and nanoscale building blocks has been widely studied and remains one of the most promising approaches for the mass manufacturing of nanomaterials.[1, 2] The ability to precisely control the assembly and organization of nanoparticles, in particular, would facilitate the highly parallel and scalable fabrication of nanomaterials with increased complexity and enhanced functionality. For example, the properties (e.g., photonic, mechanical, etc.) of nanocomposite materials may potentially be enhanced through the directed self-assembly of anisotropic nanoparticles where the resulting directionality leads to double size confinement of the rods.[3] Furthermore, the complexity and functionality of nanomaterials may also be enhanced through dissipative self-assembly, in which dynamic nanostructured materials emerge and are maintained through the dissipation of energy by entropy producing processes.[4]

Nature provides a vast number of examples where self-assembly directs the formation of materials over multiple length scales and enables diverse non-equilibrium behaviors. Here, our primary interest is in using microtubule filaments (MTs) as a model to characterize and understand the directed self-assembly of high-aspect ratio nano-arrays. MTs are biopolymer filaments formed through the polymerization of αβ tubulin dimers, resulting in hollow filaments. MTs have a diameter of ~25 nm and lengths in the tens of microns (Fig. 1A). MT filaments may be conceptualized as charged, non-interacting rigid rods (Fig. 1B), and as such, have previously been used to study the self-assembly of higher-ordered structures,[5-8] and the formation of liquid crystalline structures.[9, 10] Relevant to the present work, MTs have aspect ratios >100:1,[11] and reported persistence lengths ranging from 1 to 10 mm.[12] In addition, the net charge density of MTs has been reported at ~260 $e^- \mu m^{-1}$,[13, 14] while the α- and β-tubulin terminated ends possess positive and negative electrostatic potentials, respectively (Fig. 1B).[15] Collectively these characteristics have spurred the applications of MTs for developing functional nanomaterials[16, 17] including their use as templates for multiscale organization of metallic, magnetic, and semiconductor nanoparticles,[18-21] and for the mineralization of a range of metallic and semiconductor nanowires.[22-28]

The cyclic polymerization/depolymerization of MTs, known as dynamic instability, has been widely studied due to its physiological importance in various cellular processes.[29] Polymerization occurs from the association of αβ tubulin dimers into linear chains, called protofilaments, which subsequently associate through lateral interactions, forming a partial sheet that curls to form the mature MT filament (Fig. 1A). Energy is dissipated during polymerization through the hydrolysis of GTP on the β tubulin subunit. If the GTP is hydrolyzed prior to the addition of another dimer, however, the growing filament loses its "GTP-cap" and spontaneously depolymerizes. In addition to polymerization, previous reports have demonstrated the ability of fragmented MTs to reassemble into mature filaments. Specifically, short MT fragments generated by mechanically shearing were shown to re-form MT filaments over short timescales (i.e., minutes to a few hours) through a biomolecular annealing mechanism.[30, 31] Further characterization of this process suggested that the mechanism is diffusion controlled, with rates that are concentration dependent.[32, 33] Here we explore a related but distinct process based on the directed self-assembly of rigid nanorods (i.e., mature, intact MTs) into extended 1D nano-arrays (NAs; Fig. 1C), and show that a generalized model of rigid nano-rods may be applied to describe this self-assembly process. Using fluorescence microscopy, we demonstrate that NA self-assembly occurs over an extended period of time (at least 14 days) through a diffusion-controlled, second-order kinetic

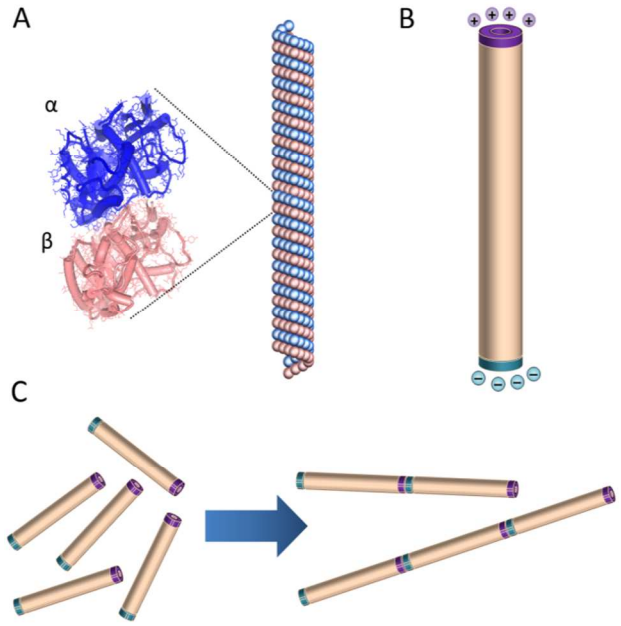

Fig. 1. (A) Crystal structure of the αβ tubulin dimer (PDB: 1JFF) and graphic representation of a mature MT filament formed through the polymerization of tubulin dimers. (B) MT filaments may be conceptualized as rigid rods in which positive and negative electrostatic potential exist at the α- and β-tubulin ends of filament, respectively. (C) Hypothesized mechanism for the head-to-tail self-assembly of MT filaments into 1D nano-arrays (NAs).

process. We further describe the mechanism of self-assembly to include the interaction of MT ends and subsequent annealing of the junction by free αβ tubulin building blocks. Overall these experiments provide a foundational understanding of directed self-assembly, and show how such assembly may be used to generate useful 1D nanostructures (e.g., nanowires) with complex structure and function.

Results and discussion

MTs primarily grow through the addition of αβ tubulin to the ends of filaments, but also may occur through annealing of sheared fragments. In the present work, we developed an approach to characterize the directed, end-to-end self-assembly of MT filaments into extended 1D NAs in which HiLyte Fluor™ 488 (HiLyte488)- and tetramethylrhodamine (TRITC)-labeled MTs were polymerized separately, stabilized with paclitaxel (i.e., Taxol®), subsequently combined, and characterized by fluorescence microscopy (Fig. 2A). The concentration of αβ tubulin in this mixture was ~0.45 μM, which is below the critical concentration for MT elongation based on the previously published phase diagram.[34] Therefore, changes in length over time may be attributable to the formation of 1D NAs via self-assembly rather than spontaneous or seeded polymerization, which occurs at higher tubulin concentrations.

Fluorescence photomicrographs qualitatively demonstrated that the length of NAs increased over the course of at least 14 days, while the number of NAs in the population decreased over this same time period (Fig. 2B). The increasing number of alternating red (TRITC) and green (HiLyte488) segments in individual NAs over time suggest that the growth is based on the directed self-assembly of individual MT filaments into arrays. If growth was attributed to nucleated polymerization rather than self-assembly, the population of filaments would have consisted of MTs with end characterized by a heterogeneous mixture of red and green tubulin, which was never observed in these experiments. It is important to note that the self-assembly of NAs also relies on the intrinsic anisotropy of the MTs, in which the different terminal protein subunits direct the head-to-tail assembly of MT filaments into NAs. The rate of growth with respect to time in diffusion-limited self-assembly/aggregation processes are known to follow power law functions.[35-37] Therefore, the increase in the average MT length (L_{NA}) over time (t in days) was quantitatively measured and fit to a power law function ($L_{NA} = 8.16 + 16.01t^{0.58}$, $R^2 = 0.99$). Here the average L_{NA} was 8.8 ± 5.0 (± SD) μm at Day 0, and increased almost ten-fold to 81.2 ± 5.0 μm at Day 14. The strong fit to the power law function suggests that the directed assembly of MT NAs is diffusion controlled, which is in agreement with annealing of MT fragments,[33] as discussed further below. As the increase in L_{NA} involves the self-assembly of two MT building blocks, a decrease in the number of MTs per field of view (N_{NA}) over time was also expected to follow a power law function and should be inversely proportional to the change in L_{NA}. Spearman rank correlation analysis confirms a strong inverse correlation between L_{NA} and N_{NA} ($\rho = -0.863$, $P < 0.001$), which further supports the end-to-end self-assembly of MTs. Therefore, the change in N_{NA} over time was fit to a power law function using negative exponent derived for L_{NA}, which yield a strong fit to the experimental data ($N_{NA} = 37.7 + 80.2t^{-0.58}$, $R^2 = 0.99$; Fig. 2C). Overall, these data demonstrate the directed self-assembly of mature MTs into larger and larger NAs occurred continuously over the course of fourteen days, which is considerably longer than prior observations with annealing of sheared MT fragments.[30, 31]

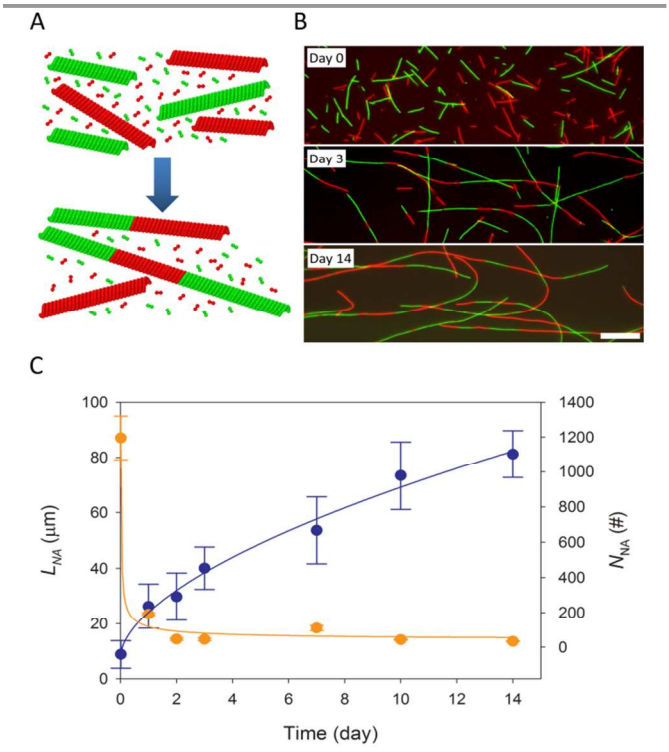

Fig. 2. (A) Graphic representation of proposed head-to-tail, directed self-assembly of TRITC (red)- and HiLyte488 (green)-labeled MT filaments to 1D NAs. (B) Time-lapse fluorescence photomicrographs showing self-assembly of red and green MTs. Scale bar = 10 μm. (C) Changes in the average NA length (L_{NA}) and average number of NAs per field of view (N_{NA}) over time. The increase in L_{NA} (–●–) and the decrease N_{NA} (–●–) over time were fit to power law functions ($L_{NA} = 8.16 + 16.01t^{0.58}$ and $N_{NA} = 37.7 + 80.2t^{-0.58}$). Error bars = standard deviation.

One may consider long-range molecular ordering in facilitating in the directed self-assembly of the 1D NAs, where the probability of end-to-end interactions by alignment of MT ends. As suggested above, MTs may be considered conceptually as non-interacting rigid rods, and therefore display liquid crystalline-like ordering following Onsager's theory,[9] where the volume fraction above which the solution phase transitions from isotropic to nematic may be defined by $\Phi^* = 4D/L$. While they are not truly rigid rods, the persistence length of MTs has been reported to be between 1 – 10 mm.[12] Similarly, MTs polymerized *in vitro* do not have a single, uniform length, but rather have lengths characterized by generalized Schulz distribution[38] due to the independent and asymmetric growth from both ends. Despite these constraints, Onsager's generalized theory can predict the liquid crystalline ordering of MT solutions.[9] For a population of MTs with an average length of 8.8 μm (i.e., starting average length in this experiment), the solution should be in a nematic phase when Φ_V^{MT} is greater than ~0.011. The density of MTs can be estimated at ~2 x 10^{10} MTs mL^{-1} based on the mass of tubulin and final volume used for our experiments. The volume of a single MT with an average length of 8.8 μm is ~4.3 x 10^{-15} mL. Using this value, Φ_V^{MT} may be estimated to be ~0.00008, more than 100-fold less than the critical concentration necessary for spontaneous ordering. Thus, MT solutions used in these experiments were isotropic, suggesting that the directed assembly of filaments was likely not driven by end-to-end stacking induced by liquid crystal ordering. The density of MTs over time, however, is maintained in a regime where collisions should be frequent (i.e., $>L^{-3}$) and therefore should play a critical role in the self-assembly of MTs.

As noted above, significant changes in L_{NA} (~3-fold increase) and N_{NA} (6-fold decrease) were observed as early as one day after initiation of MT self-assembly. To better characterize the rate of self-assembly, a second set of experiments were performed to measure changes in L_{NA} and N_{NA} on a shorter timescale (i.e., less than 24 hr). Here, self-assembly of NAs of TRITC and HyLite488 MTs was observed as soon as 15 min post-mixing of the two populations of paclitaxel-stabilized filaments, and became increasingly predominant over time (Fig. 3A). These results agree with the previously published observations of length redistribution of MTs as soon as fifteen minutes post-shearing into fragments.[33] The data for L_{NA} between $t = 0$ and $t = 24$ hr were plotted and fit to a power law function, yielding $L_{NA} = 2.96 + 1.37t^{0.76}$ ($R^2 = 0.97$; Fig. 3B). The average NA length at $t = 0$ was 2.2 ± 0.2 μm and increased more than eight-fold to 18.9 ± 2.6 μm at $t = 24$ hr. The average N_{NA} concurrently decreased over time and was fit to a power law function based on $t^{-0.76}$ ($N_{NA} = 110.47 + 89.14t^{-0.76}$, $R^2 = 0.74$). Spearman correlation analysis of the data

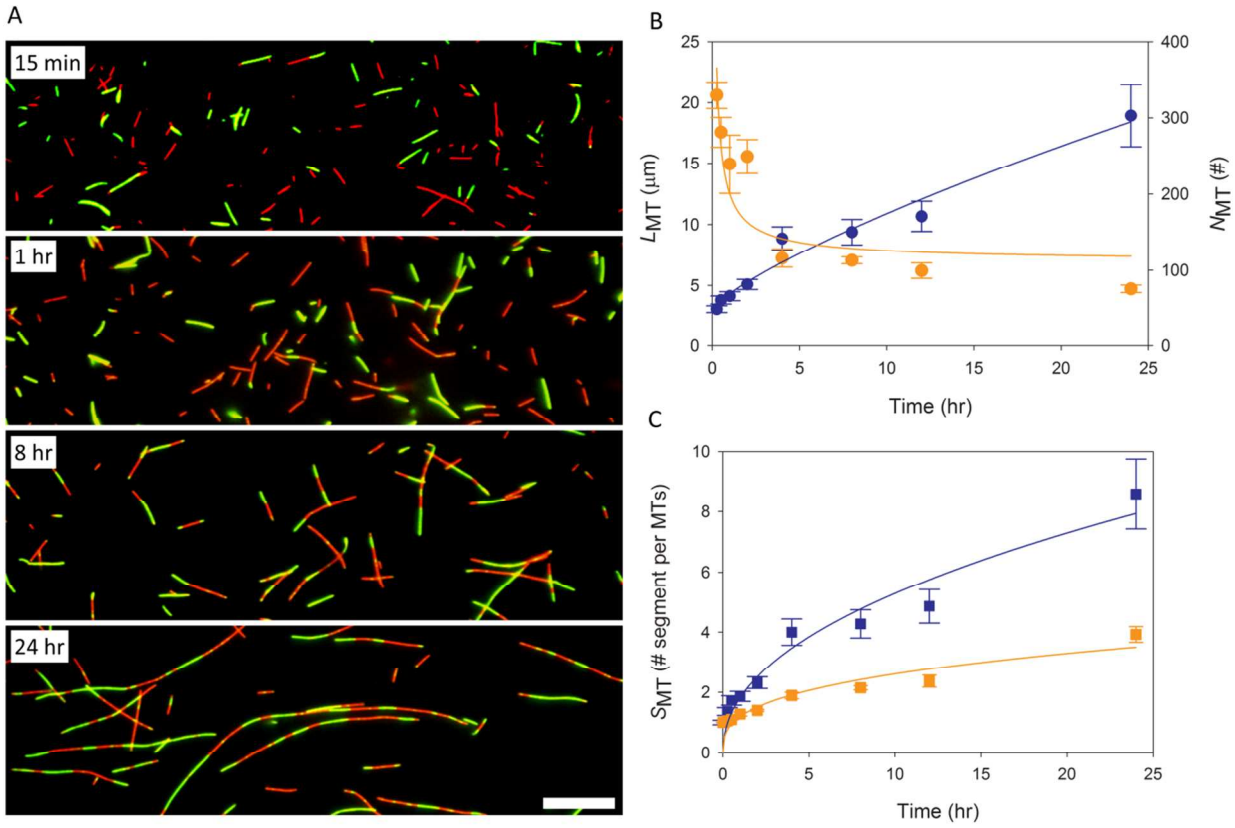

Fig. 3. (A) Fluorescence photomicrographs showing end-to-end self-assembly of TRITC (red)- and HiLyte488 (green)-labeled MT filaments at four different time points. Scale bar = 10 μm. (B) The end-to-end self-assembly of MTs, as measured by a change in length (L_{NA}, –●–) and the number of MTs per field of view (N_{NA}, –●–) over the course of seven days. L_{NA} and N_{NA} were fit with a power law functions where $L_{NA} = 2.96 + 1.37t^{0.76}$ and $N_{NA} = 110.47 + 89.14t^{-0.76}$), respectively. (C) The number of segments per MT (S_{NA}) was determined by either (*i*) counting the number of alternating red-green segments in a MT (–■–) or (*ii*) dividing the MT length at a given time point by the starting length (–■–). For both methods, the change in S_{NA} was fit to a power law function ($S_{NA} = 1.19t^{0.34}$; and $S_{NA} = 1.82t^{0.46}$, respectively).

indicated a significant inverse correlation between L_{NA} and N_{NA} (ρ = -0.983, P < 0.001). Collectively these data were consistent with the observations for longer time periods, and suggest that directed self-assembly at both short and long timescales is diffusion controlled.

The rate of self-assembly in this experiment was further characterized by determining the number of MT segments per NA (S_{NA}) over time. S_{NA} was first measured empirically by counting the number of red and green segments present in each NA, plotted as a function of time (Fig. 3C, orange line), and fit to a power law function ($S_{NA} = 1.19t^{0.34}$; $R^2 = 0.78$). If one considers the assembly process, however, assembly of two MTs into a NA can involve (1) two green MTs, (2) two red MTs, or (3) one red and one green MT, with event distributions approximating 25%, 25%, and 50%, respectively. These distributions assume an unbiased self-assembly event where specific interactions (e.g., green-green assembly) are not favored. Accordingly, determining S_{NA} by counting MT segments likely underestimates the number events over time and overall rate of self-assembly, perhaps by as much as 50%. As an alternate approach, S_{NA} was estimated by dividing the length of a NA at a given time by the average starting length (Fig. 3C, blue line). Plotting S_{NA} over time also fits well to a power law function with $S_{NA} = 1.82t^{0.46}$ ($R^2 = 0.93$). Here the coefficient of this expression is approximately 1.5-fold greater than that derived from simply counting the number of red/green segments. Further, NAs at t = 24 hr were composed of an average of approximately eight MT segments based on the second method, which is approximately twice the number of MT segments (i.e., ~four per MT NA) as determined using the initial counting method (Fig. 3C).

The kinetics of self-assembly was next determined by estimating the percent of "monomers" (P_m) in a population of NAs over time, where a monomer was defined as a MT that possessed only a single fluorescent dye (i.e., a MT had not self-assembled into a NA). Two experimental populations were prepared for these experiments: (1) HiLyte488- and TRITC-MTs with free GTP-tubulin dimers, and (2) HiLyte488- and TRITC-MTs alone (i.e., little to no free GTP- tubulin dimers). The latter population was prepared by cyclic centrifugation to remove of the majority, but likely not all, of unpolymerized GTP-tubulin. In these experimental populations, P_m decreased exponentially as a function of time (Fig. 4A), where $P_m = 93.1e^{-0.11t}$ ($R^2 = 0.94$) for MTs with GTP-tubulin dimers, and $P_m = 97.1e^{-0.09t}$ ($R^2 = 0.97$) for MTs alone. Plotting the inverse of P_m over of time yielded linear relationships for both populations (Fig. 4B), indicating the directed assembly proceeds according to second-order reaction kinetics. The rates of assembly for MTs + GTP-tubulin and MTs alone were estimated as $1/(P_m) = 0.0095 + 6.2 \times 10^{-7}t$ ($R^2 = 0.97$) and $1/(P_m) = 0.0102 + 4.3 \times 10^{-7}t$ ($R^2 = 0.99$), respectively (where t is in seconds). It should be noted that, based on the prior discussion, these rates are likely an underestimate of the actual rates as the assembly of like-colored MTs into NAs cannot be discerned. Here the data demonstrate that reduction in the concentration of free GTP-tubulin dimer in solution results in a ~30% reduction in the rate of NA self-assembly, suggesting that it may potentially play an important role in this process. The rate of annealing by sheared MTs fragments has also been reported to follow second-order kinetics,[31, 32, 39] despite suggestions that the other factors (e.g., long-range ordering and reduced diffusion) preclude second order kinetics.[30, 33] In contrast, we observed self-assembly of 1D NAs in isotropic solutions that is diffusion-limited (Fig. 2C and 3B) and follows second-order rate kinetics (Fig. 4B).

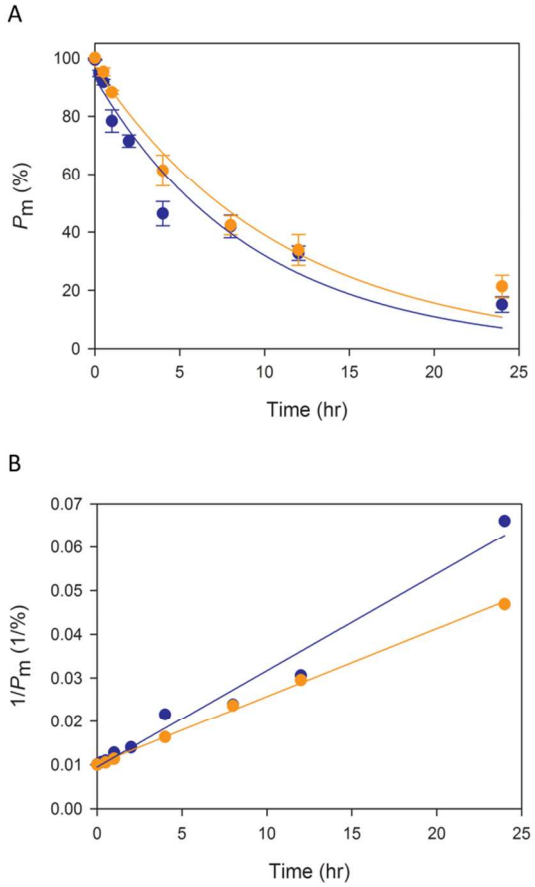

Fig. 4. (A) The percent of monomers in populations of MTs and GTP-dimers (–●–) and MT alone (–●–) follow an exponential decay as a function of time ($P_m = 93.1e^{-0.11t}$ and $P_m = 97.1e^{-0.09t}$, respectively). (B) Plotting the inverse of P_m as a function of time yielded linear relationships for both populations (MTs + GTP-tubulin, $1/(P_m) = 0.0095 + 6.2 \times 10^{-7}t$; MT alone, $1/(P_m) = 0.0102 + 4.3 \times 10^{-7}t$), indicative that the end-to-end assembly proceeds according to a second-order reaction rate.

A key aspect of self-assembly in our system involves the formation of junctions between the individual MTs in the NAs. Based on the data regarding excess GTP-tubulin and rate kinetics, we hypothesized that the self-assembly mechanism involved two steps, one of which required GTP-tubulin for high-fidelity self-assembly. In an idealized mechanism, such as depicted in Fig. 1, two blunt-ended MTs are able to form a stable end-to-end junction and self-assemble in a single step. While MT ends may be blunt, additional morphologies, such as tapered ends and curved sheets, exist at α and β ends of a MT filament.[40-42] In the absence of blunt ends, considerable lattice mismatch and vacancies will likely exist at the junction between MTs ends. Therefore, we hypothesized that NA self-assembly followed a two-step process (Fig. 5A) in which either: (*i*) blunt ends are formed by the addition of free GTP-tubulin to MT ends prior to assembly, or (*ii*) lattice vacancies associated with junctions formed by tapered MT ends are filled by the addition of free GTP-tubulin in these junctions. In the latter scenario, MT ends may temporarily bind through attractive electrostatic interactions and/or hydrophobic interactions,[15] but require recruitment of GTP-tubulin dimers to fill lattice vacancies, enable correct lattice matching, and form a stable junction.

The hypothesized two-step mechanism was tested using a solution containing green MT filaments to which free red tubulin dimers were added. More specifically, we characterized the formation of junctions in NAs using HyLite488 MTs that were isolated by centrifugation and suspended with a solution containing free TRITC GTP-tubulin. If lattice vacancies existed at these junctions and were eliminated through recruitment of free GTP-dimers from solution, we would expect to observe 1D NAs with short section of red tubulin between the individual green MT segments (Fig. 5B). At t = 0, only green MTs were observed within the population suggesting that the solution was free of TRITC-labeled MTs (Fig. 5B, Day 0). Moreover, the concentration of free TRITC GTP-tubulin in these experiments was below the threshold for spontaneous nucleation and growth of MTs.[34] As soon as one day after initiation, assembled NAs composed of green segments joined by short red segments were observable within the population (Fig. 5B). Close examination also revealed the presence of short, red ends on a number of the assembled NAs, suggesting that a certain level of seeded polymerization occurred in these experiments. Here the use of different fluorescent tubulins provided a novel approach to visualize the junctions between MTs in the arrays, an aspect that had not been described in prior studies of annealing by sheared MT fragments.

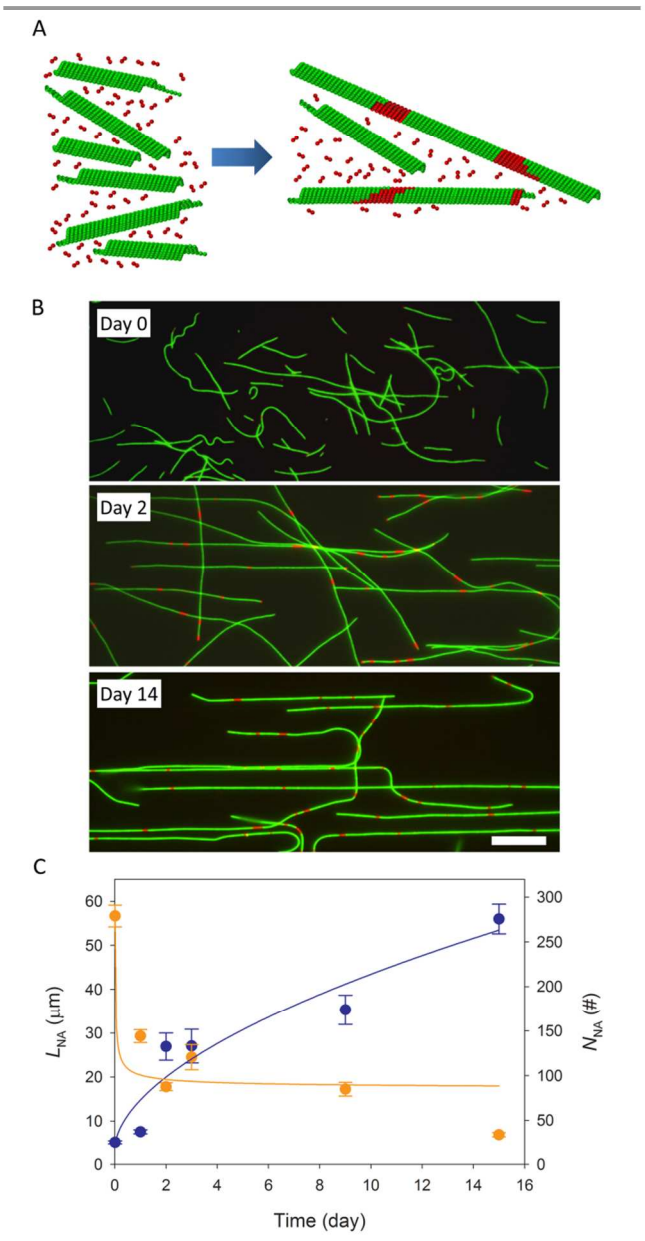

Fig. 5. (A) Artistic representation and (right) fluorescence photomicrographs of end-to-end self-assembly of HiLyte488-labeled MT filaments in the presence of unpolymerized TRITC tubulin dimers (left). (B) Time-lapse fluorescence photomicrographs representing typical observations over NA self-assembly over time. Scale bar = 10 μm. (C) The increase in L_{NA} (–●–) and decrease in N_{NA} (–●–) were both fit to power law functions where $L_{NA} = 3.65 + 11.12t^{0.55}$ and $N_{NA} = 84.99 + 15.66t^{-0.55}$).

As with prior experiments, the growth of NAs was quantitatively measured by the changes in length and MT concentration over time. Increases in L_{NA} and decreases in N_{NA} were fit to power law functions (Fig. 5C) as described above, and yielded consistent fits with the data ($L_{NA} = 3.65 + 11.12t^{0.55}$, $R^2 = 0.91$; $N_{NA} = 84.99 + 15.66t^{-0.55}$, $R^2 = 0.84$). In addition, an inverse correlation was observed between L_{NA} and N_{NA} ($\rho = -0.943$, P = 0.02), confirming that NA elongation in this experimental system was primarily due to self-assembly and not seeded polymerization. Overall the data obtained in this experiment support our proposed mechanism in which free GTP-tubulin is required to either form blunt ends prior to assembly, or to fill lattice vacancies following alignment and interaction of tapered MT ends. These two mechanisms are not mutually exclusive, and it is possible that NA self-assembly involves both mechanisms.

Due to the resolution limitations of optical microscopy, molecular dynamics simulations (MD) of our coarse-grained MT model[43, 44] was used to investigate the self-assembly and formation of junctions formed by blunt- or tapered-ended MTs. In initial simulations, we used pre-assembled MTs composed of tubules with thirteen protofilaments and L = 10 monomers long, where a "monomer" represented the αβ tubulin dimer. Fig. 6A shows a time-lapse sequence from a simulation in which two blunt-ended MTs diffuse close together, followed by alignment of the opposing ends and finally assembly into a NA. While these simulations use relatively small tubules, the sequence of events should take place regardless of starting tubule, length and hold true for micron-scale MT filaments. The simulations also show that the vertical interaction strength (A_V) of 2.6 kT is sufficient to produce a stable junction between two self-assembled, blunt-ended MTs. One of the central questions in NA self-assembly is the likelihood of two MT ends finding each other with the right orientation for adhesion and junction formation. While the simulations allow for the observation of individual self-assembly events for short tubules, assembly of NAs formed by multiple events or assembly of NAs from large (e.g., micron-sized) tubule cannot be generated with our model. Specifically, the time scales for each assembly event increases based on the aspect ratio of the tubule, as the probability of two MTs becoming aligned end-to-end significantly decreases as a function of MT length. Thus, the time scale becomes prohibitively long for simulations, even for L → 3L. Regardless of this limitation, the simulations do confirm our hypothesis that blunt-ended MTs are able to self-assemble into 1D NAs through the formation of stable junctions between opposing ends of two tubules.

We also performed MD simulations on a system that has MTs with tapered (incomplete) ends and free monomers. For tapered ends, when two MTs come together, the binding energy is initially reduced as the number of binding monomer pairs is

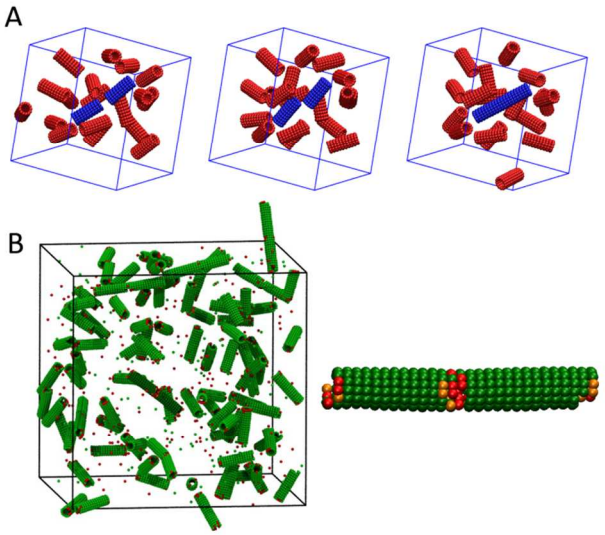

Fig. 6. (A) Images of a pair (blue) of MTs self-assembling to form a single 1D NA from a simulation of blunt-end tubules, without free monomers, and with tubules with L = 10, A_L = 4.4 kT and A_V = 2.6 kT. (B) (left) Image from MD simulation of the self-assembly of tapered-ended MTs (green) in the presence of free monomers (red). The assembled NA near the center (colored dark green) is shown at higher resolution to the right of the simulation box. In this image, orange-colored monomers represent monomers that dissociated from another MT and red-colored monomers were free in solution prior to binding. Both monomer types fill lattice vacancies at junctions in the NA, as well as add to the ends of NAs. The starting parameters were L = 13.5, A_L = 4.4 kT, and A_V = 3.3 kT.

reduced. Here we observed that free monomers can bind to the MT ends (i.e., seeded polymerization) before self-assembly, thus smoothing the end for better adhesion and junction formation (Fig. 6B). In addition, we observed that some of the monomers at the tapered ends of the MTs detach (depolymerize) and subsequently rebind to other MTs. In the simulations, the concentration of these detached monomers is likely greater than in the experiments, as the simulations are performed using a higher concentration to speed up the dynamics. We further observed that free monomers are able to fill in lattice vacancies following initial assembly and stabilize the junction between opposing ends. The image in Fig. 6B (right) displays one example in which two tapered-ended MTs align and self-assemble into an NA, but gaps remains at the junction between the two MTs. Free monomers fill in these lattice defects and stabilize the junction, which supports our earlier hypothesis. This observation is consistent with the tapered ends possessing a lower binding energy (i.e., limited ability to maintain a junction), and the addition of the free monomers to these defect sites, which stabilizes the self-assembled junction. Collectively the data from our MD simulations support the contention that free GTP-tubulin plays a critical role in removing defects either before (forming blunt-ended MTs) or after (vacancy filling) self-assembly of MTs into NAs.

Conclusions

Directed self-assembly of nanomaterials has the potential to significantly enhance our ability to create mesoscopic materials that are highly complex and display unique functionality. Here we have demonstrated that rigid polymer rods will self-assemble into extended 1D NAs following second-order rate kinetics, which can be maintained over an extended period of time (e.g., weeks). We attribute the directed, longitudinal self-assembly, at least in part, to the inability of MTs to assemble laterally due to electrostatic repulsion, as well as electrostatic attraction and hydrophobic interactions between opposing ends of the MTs.[15, 45] In our system, both the size and chemical nature of the segments within the assembled NAs may be easily modified by engineering the starting length of the filaments[38] and polymerizing MT building blocks with different compositions of tubulin dimers.[21] The latter aspect (i.e., varying chemical composition) enables the subsequent application of these heterostructured NAs as templates for segment-selective biomineralization and/or nanoparticle deposition, forming novel multi-functional nanowires.[17] More broadly, the knowledge gained from these experiments provide valuable insights with regard to designing relatively simple nano-rods that are capable of directed assembly into more structurally and functionally complex 1D assemblies.

In summary, we have described the directed self-assembly of MT filaments into extended 1D NAs based on a generic model broadly applicable to rigid nano-rods. Using this simple system, we demonstrate that MT building blocks will undergo spontaneous, prolonged self-assembly over the course of at least fourteen days, leading to the formation of NAs with aspect ratios exceeding 3,000:1. We further show that the intrinsic properties of MTs (i.e., attractive ends) are crucial in achieving head-to-tail assembly, and that the addition of αβ tubulin dimers at segment interfaces eliminate lattice vacancies and stabilize junctions. The fundamental knowledge established in these studies may be applied directly for generating MT templates for biomineralization of complex nanostructures, as well as more broadly for the direct self-assembly of nano-rods and wires into functional 1D mesostructures.

Experimental Section

Preparation of MTs and motor proteins

TRITC, and HiLyte488-labeled porcine tubulin were purchased from Cytoskeleton, Inc. (Denver, CO). MTs were prepared by rehydrating lyophilized tubulin in BRB80 buffer (80 mM PIPES pH 6.9, 1 mM MgCl2, 1 mM EGTA) containing 1 mM GTP and 10% glycerol (5 mg mL^{-1} final tubulin concentration, and polymerizing at 37°C for 25-30 minutes. The polymerized MTs were then stabilized by diluting 100-fold into BRB80T (BRB80 with 10 μM paclitaxel) for a final tubulin concentration of ~0.9 μM.

To measure the amount of tubulin that was not incorporated into MTs, solutions were centrifuged at 25,000 x g for 2 hr, and the pellet containing polymerized MTs was suspended in 100 μL BRB80T; the supernatant containing unpolymerized tubulin was also saved. The ratio of polymerized to unpolymerized tubulin was then characterized by polyacrylamide gel electrophoresis (PAGE), and suggested that 50-60% of the tubulin was incorporated into MTs (*not shown*).

A kinesin-1 motor protein from *Drosophila melanogaster* was used to bind MTs to the surfaces of a glass flow cell and facilitate characterization of fused MTs. The histidine-tagged kinesin heavy chain motor was prepared by expressing the pPK113 plasmid[46] in Escherichia coli BL21 (DE3) pLysS. When the culture reached an OD600nm of ~0.7, protein expression was induced by addition of isopropylthio-β-

galactoside (IPTG) to final concentration of 0.5 mM. Cells were harvested by centrifugation at 9,000 x g, flash frozen in liquid nitrogen, and stored at -80°C until used. Cells were lysed using BugBuster® with Benzonase,® (EMD BioSciences, Inc., Billerica, MA) and AEBSF (Calbiochem®. EMD Millipore, Darmstadt, Germany), and kinesin was then purified on a Ni-NTA column as previously described.[21, 46]

Self-assembly characterization

For initial characterization of end-to-end assembly and formation of 1D NAs, TRITC and HyLite tubulin were polymerized and stabilized with BRB80T as described above. The two separate populations were then combined together and stored at room temperature. Inverted kinesin-MT assays were performed by constructing flow cells using a microscope slide, double-sided tape and a #1 glass coverslip. Casein (0.5 mg mL-1 in BRB80) was incubated in the flow cell for 5 min, followed by a solution of kinesin (~5 nM in BRB80 with 0.2 mg mL^{-1} casein and 1 mM AMP-PNP). MTs were then infused into the flow cell with 1 mM AMP-PNP in BRB80T containing anti-fade reagents,[21] and allowed to bind to the kinesin-coated surface for 10 min. After incubation, the flow cell was washed with the BRB80 + AMP-PMP solution to remove unbound any unbound MTs. Characterization of the NAs was performed by epifluorescence using an Olympus IX71 microscope and Hamamatsu ORCA 3CCD camera. Still-frame images were taken on Days 0, 1, 2, 3, 6, 9, and 14. The lengths (L_{NA}) of at least fifty NAs per treatment and time point were measured using the Neurite Tracing[47] function in Fiji.[48] The number of NAs in a field of view, for each of ten fields of view, was determined for all treatments and at each time point. Curve fitting and statistical analyses were performed using SigmaPlot 12.5 (Systat Software, San Jose, CA).

A similar approach as outlined above was used to characterize the rate and kinetics of NA self-assembly. Separate populations of TRITC and HyLite MTs were polymerized as described above, subsequently combined together, and incubated at room temperature. Assembly was analyzed by epifluorescence microscopy of NAs bound to kinesin-coated glass slides at various time points between $t = 0$ and $t = 24$ hr. The number of red and green segments in each NA, the length of each NA, and the number of NAs per field were measured at each time point, as described above. In addition, the rate of assembly was characterized by counting the number of "monomers" (P_m), which we defined as a MT composed of only a single color, in a field of view at each time point. To understand the effect of free GTP-tubulin on NA self-assembly, populations of TRITC and HyLite MTs were prepared in which centrifugation was used to remove the majority of unpolymerized GTP-tubulin from solution prior to assembly. Pellets containing MTs were gently suspended in BRB80T, combined together, and incubated at room temperature. Images were collected and analyzed as described above.

The hypothesized mechanism of NA self-assembly was tested using a combination of HyLite MTs and TRITC GTP-tubulin. Here, separate populations of TRITC and HiLyte tubulin were polymerized at 37°C for 25-30 min, as described above, and stabilized in 100 µL of BRB80T. The polymerized MTs were then centrifuged at 25,000 *x g* for 2 hr at room temperature. Supernatant from HiLyte MT solution was removed and discarded, while the pellet was suspended with 10 µL of BRB80T. The supernatant from the TRITC MTs was transferred to a new microcentrifuge tube and incubated at 4°C for 30 min to depolymerize any short MTs. The suspended HiLyte MT pellet was then added to 90 µL of the TRITC supernatant, following equilibration to room temperature. Characterization and analysis of MT self-assembly was performed as described above.

Molecular dynamics simulations

Molecular dynamics (MD) simulations of a simple MT model were used to provide further understanding of directed, end-to-end assembly. Complete details regarding the simulation setup may be found in our previous work.[43, 44] Briefly, the "monomer" representing the αβ tubulin dimer possesses a a wedge shape and composed of 27 particles (3 x 3 x 3), which only have purely repulsive interactions that give the monomer its shape. Two attractive sites per surface are located on the top and bottom, and the lateral sides and enable self-assembly of monomers into tubules that mimic that of real MTs. Previous work has shown that the monomers will self-assemble into tubules with the appropriate vertical interactions strength (A_V) and lateral interaction strength (A_L). For the present work, pre-assembled nonhelical tubules of length L monomers and thirteen protofilaments were randomly placed in the simulation cell with additional NF free monomers. Standard constant temperature molecular dynamics simulations were then performed to study the directed self-assembly of the tubules over time.

Acknowledgements

We sincerely thank Drs. Erik Spoerke and Darryl Sasaki for their insightful comments and discussions regarding the content of this manuscript. This research was supported by the U.S. Department of Energy, Office of Basic Energy Sciences, Division of Materials Sciences and Engineering, Project KC0203010. Sandia National Laboratories is a multi-program laboratory operated by Sandia Corporation, a wholly owned subsidiary of Lockheed Martin company, for the U.S. Department of Energy's National Nuclear Security Administration under contract DE-AC04-94AL85000.

Notes and references

[a] Department of Nanobiology, Sandia National Laboratories, Albuquerque, NM 87185, USA.
[b] Center for Integrated Nanotechnologies, Sandia National Laboratories, Albuquerque, NM 87185-1303, USA. E-mail: gdbacha@sandia.gov; Fax: +1 (505) 284-7778; Tel: +1 (505) 844-5164.
[c] Department of Computational Materials and Data Science, Sandia National Laboratories, Albuquerque, NM 87185, USA.
[d] Present address: Department of Physics, Virginia Polytechnic Institute and State University, Blacksburg, Virginia 24061, USA.

1. B. A. Parviz, D. Ryan and G. M. Whitesides, *IEEE Trans. Adv. Packag.*, 2003, **26**, 233-241.
2. G. M. Whitesides and B. Grzybowski, *Science*, 2002, **295**, 2418-2421.
3. K. Liu, N. Zhao and E. Kumacheva, *Chem. Soc. Rev.*, 2011, **40**, 656-671.
4. M. Fialkowski, K. J. M. Bishop, R. Klajn, S. K. Smoukov, C. J. Campbell and B. A. Grzybowski, *J. Phys. Chem.B*, 2006, **110**, 2482-2496.
5. S. Aoyama, M. Shimoike and Y. Hiratsuka, *Proc. Natl. Acad. Sci. U. S. A.*, 2013, **110**, 16408-16413.
6. L. Hamon, P. Savarin, P. A. Curmi and D. Pastre, *Biophys. J.*, 2011, **101**, 205-216.
7. D. J. Needleman, M. A. Ojeda-Lopez, U. Raviv, H. P. Miller, L. Wilson and C. R. Safinya, *Proc. Natl. Acad. Sci. U. S. A.*, 2004, **101**, 16099-16103.

8. I. S. Aranson and L. S. Tsimring, *Phys. Rev. E*, 2006, **74**, 031915−1-15.
9. A. L. Hitt, A. R. Cross and R. C. Williams, *J Biol Chem*, 1990, **265**, 1639-1647.
10. M. V. Sataric and J. A. Tuszynski, *Phys. Rev. E*, 2003, **67**, 011901−1-11.
11. A. Desai and T. J. Mitchison, *Annu. Rev. Cell Dev. Biol.*, 1997, **13**, 83-117.
12. T. Hawkins, M. Mirigian, M. S. Yasar and J. L. Ross, *J. Biomech.*, 2010, **43**, 23-30.
13. T. Kim, M. T. Kao, E. F. Hasselbrink and E. Meyhofer, *Biophys. J.*, 2008, **94**, 3880-3892.
14. R. Stracke, K. J. Bohm, L. Wollweber, J. A. Tuszynski and E. Unger, *Biochem. Bioph. Res. Commun.*, 2002, **293**, 602-609.
15. N. A. Baker, D. Sept, S. Joseph, M. J. Holst and J. A. McCammon, *Proc. Natl. Acad. Sci. USA*, 2001, **98**, 10037-10041.
16. G. D. Bachand, N. F. Bouxsein, V. VanDelinder and M. Bachand, *Wiley Interdiscip. Rev.-Nanomed. Nanobiotechnol.*, 2014, **6**, 163-177.
17. K. C.-W. Wu, C.-Y. Yang and C.-M. Cheng, *Chem. Commun.*, 2014, **50**, 4148-4157.
18. E. D. Spoerke, A. K. Boal, G. D. Bachand and B. C. Bunker, *ACS Nano*, 2013, **7**, 2012-2019.
19. M. Achermann, S. Jeong, L. Balet, G. A. Montano and J. A. Hollingsworth, *ACS Nano*, 2011, **5**, 1761-1768.
20. M. Platt, G. Muthukrishnan, W. O. Hancock and M. E. Williams, *J. Amer. Chem. Soc.*, 2005, **127**, 15686-15687.
21. G. D. Bachand, S. B. Rivera, A. K. Boal, J. Gaudioso, J. Liu and B. C. Bunker, *Nano Letters*, 2004, **4**, 817-821.
22. A. K. Boal, T. J. Headley, R. G. Tissot and B. C. Bunker, *Adv. Funct. Mater.*, 2004, **14**, 19-24.
23. S. Behrens, J. Wu, W. Habicht and E. Unger, *Chem. Mater.*, 2004, **16**, 3085-3090.
24. J. C. Zhou, Y. Gao, A. A. Martinez-Molares, X. Y. Jing, D. Yan, J. Lau, T. Hamasaki, C. S. Ozkan, M. Ozkan, E. Hu and B. Dunn, *Small*, 2008, **4**, 1507-1515.
25. Y. Yang, B. H. Constance, P. A. Deymier, J. Hoying, S. Raghavan and B. J. J. Zelinski, *J Mater Sci*, 2004, **39**, 1927-1933.
26. K. Valenzuela, S. Raghavan, P. A. Deymier and J. Hoying, *J. Nanosci. Nanotechnol.*, 2008, **8**, 3416-3421.
27. R. Kirsch, M. Mertig, W. Pompe, R. Wahl, G. Sadowski, K. J. Bohm and E. Unger, *Thin Solid Films*, 1997, **15**, 1-2.
28. E. D. Spoerke, B. A. Connor, D. V. Gough, B. B. McKenzie and G. D. Bachand, *Part. Part. Syst. Charact.*, 2014, **31**, DOI: 10.1002/ppsc.201400013.
29. T. E. Holy and S. Leibler, *Proc. Natl. Acad. Sci. U. S. A.*, 1994, **91**, 5682-5685.
30. S. W. Rothwell, W. A. Grasser, H. N. Baker and D. B. Murphy, *J. Cell Biol.*, 1987, **105**, 863-874.
31. S. W. Rothwell, W. A. Grasser and D. B. Murphy, *J. Cell Biol.*, 1986, **102**, 619-627.
32. R. C. Williams and L. A. Rone, *Protoplasma*, 1988, **145**, 200-203.
33. R. C. Williams and L. A. Rone, *J. Biol. Chem.*, 1989, **264**, 1663-1670.
34. D. K. Fygenson, E. Braun and A. Libchaber, *Phys Rev E*, 1994, **50**, 1579-1588.
35. J. R. Rothenbuhler, J.-R. Huang, B. A. DiDonna, A. J. Levine and T. G. Mason, *Soft Matter*, 2009, **5**, 3639.
36. E. Climent, M. R. Maxey and G. E. Karniadakis, *Langmuir*, 2004, **20**, 507-513.
37. T. Savin and P. S. Doyle, *Soft Matter*, 2007, **3**, 1194-1202.
38. Y. Jeune-Smith and H. Hess, *Soft Matter*, 2010, **6**, 1778-1784.
39. M. Caplow, J. Shanks and B. P. Brylawski, *J Biol Chem*, 1986, **261**, 6233-6240.
40. D. Chretien, S. D. Fuller and E. Karsenti, *J. Cell Biol.*, 1995, **129**, 1311-1328.
41. T. Muller-Reichert, D. Chretien, F. Severin and A. A. Hyman, *Proc. Natl. Acad. Sci. U. S. A.*, 1998, **95**, 3661-3666.
42. E. M. Mandelkow, E. Mandelkow and R. A. Milligan, *J. Cell Biol.*, 1991, **114**, 977-991.
43. S. Cheng and M. J. Stevens, *Soft Matter*, 2014, **10**, 510-518.
44. S. Cheng, A. Aggarwal and M. J. Stevens, *Soft Matter*, 2012, **8**, 5666-5678.
45. E. Nogales, M. Whittaker, R. A. Milligan and K. H. Downing, *Cell*, 1999, **96**, 79-88.
46. D. L. Coy, M. Wagenbach and J. Howard, *J. Biol. Chem.*, 1999, **274**, 3667-3671.
47. M. H. Longair, D. A. Baker and J. D. Armstrong, *Bioinformatics*, 2011, **27**, 2453-2454.
48. J. Schindelin, I. Arganda-Carreras, E. Frise, V. Kaynig, M. Longair, T. Pietzsch, S. Preibisch, C. Rueden, S. Saalfeld, B. Schmid, J. Y. Tinevez, D. J. White, V. Hartenstein, K. Eliceiri, P. Tomancak and A. Cardona, *Nat. Methods*, 2012, **9**, 676-682.

